Fluctuation-dissipation model for synthesis of superheavy elements

Y. Aritomo, T. Wada, and M. Ohta
Department of Physics, Konan University, Kobe, Hyogo 658-8501, Japan

Y. Abe
YITP, Kyoto University, Kitashirakawa, Kyoto 606-8501, Japan

(Received 4 June 1998)

Fusion-fission dynamics in superheavy elements is investigated by an approximate fluctuation-dissipation model, i.e., a diffusion model in the deformation space, assuming that the kinetic energy of the incident ion dissipates immediately after the contact. The probability accumulated inside the fission barrier is calculated by the one-dimensional Smoluchowski equation taking account of the temperature dependence of the shell correction energy. A new mechanism for an optimum condition is found as a compromise of two conflicting requirements: higher incident energy for larger fusion probability and lower excitation energy of compound nuclei for larger survival probability. Enhancements of the residue cross sections at the optimum condition are obtained for the cases in which the cooling is quick to restore the shell correction energy, combined with slow fissioning motion due to the strong friction. With symmetric combinations of incident ions, the (HI, 3-4n) channels show the enhancement. [S0556-2813(99)01501-0]

PACS number(s): 25.70.Jj, 24.60.Ky, 24.60.Dr, 27.90.+b

I. INTRODUCTION

Atomic nuclei which have closed shell structures are known to be unusually stable, as observed in the natural abundance, etc. Following Strutinski's idea [1,2], the stability is given by the shell correction energy which is easily and rather reliably calculated from the single-particle spectrum of nucleus. Extensions of such calculations to heavier, naturally nonexistent nuclides have predicted superheavy elements to be stable against fission around the double-closed-shell nucleus with $Z=114$ and $N=184$ [3–8]. Many-body calculations with the mean field approximation [9,10] also have predicted such a high stability in the same region of the nuclear chart, though some of them predict the proton shell closure in even heavier elements like $Z=120$ or 126. Naturally the theoretical predictions are to be confirmed by experiments, i.e., by synthesizing them.

Attempts for synthesizing heavy elements beyond the atomic number $Z\sim100$ have become active since the 1970s by means of various developments in experimental techniques [11–13], and have recently succeeded in identifying the element $Z=112$ [14], which gives us hope to reach the element 114.

The method of the so-called *cold fusion* [13,15], in which the excitation energy of the compound nucleus is suppressed to a minimum ($E^*\leqslant20$ MeV) so as to inhibit multichance fission and to consequently gain the yield of evaporation residue products, has attracted attention. The magic nucleus ^{208}Pb or ^{209}Bi was used as a target to produce the series of heavy elements up to $Z=112$ [11,14,16–20], but the cross sections are extremely small with the order of pb for the elements 111 and 112 due to small fusion probabilities. Empirically cross sections for $Z>112$ are expected to be even smaller.

For superheavy elements around $Z\sim114$ and $N\sim184$, practical combinations of target and projectile, such as ^{244}Pu+^{48}Ca, would lead to compound nuclei at rather high excitation. There is a discussion based on the different approach that the combination of the most stable projectile and target as an entrance channel may be favorable for superheavy element synthesis with the cold fusion mechanism [21]. Naturally, however, their approach does not take into account the effects of dissipation and fluctuation in the reaction mechanism. In the future, more mass-symmetric combinations which lead to lower excitations are expected to be available at new facilities such as proposed in the PIAFE project [22,23]. Although in heavier systems fusion hindrance is known to exist as expressed in the necessity of extra-push or extra-extra-push energy, it is thus natural to explore the possibility in this direction, so-called *hot fusion*, in which higher incident energies are used to gain much larger fusion probabilities in spite of the hindrance, and thereby the compound nuclei formed are in rather high excitation, say, $E^*\sim40$ MeV. They are accompanied by undesirable high fission probabilities. It nevertheless seems to be meaningful, because the fission of highly excited nuclei has been clarified to be much hindered [24,25]. Actually, it is observed experimentally that prescission neutron multiplicities increase as a function of excitation energy [26,27], while postscission ones do not. This means that most of the excitation energies are carried away by neutrons and the compound nuclei are cooled down before fission. This is well explained by dissipative dynamical calculations of fissioning motion with strong friction such as given by the one-body wall-and-window formula [28,29]. Therefore, fission is expected to be far slower than the prediction of the conventional Bohr-Wheeler theory. The decrease of residue cross sections by fission in higher excitation is thus reduced and could be covered or overcovered by an increase of fusion probability.

Although there have been enormous experimental efforts as stated above [30], they are more or less empirical, and theoretical developments are still insufficient. Of course, static properties such as potential energy surface including

the shell and the pairing correction energies are investigated quite in detail and decays of assumed compound nuclei are analyzed very carefully with the statistical model [31], but formation processes yet remain to be studied in the superheavy mass region. In other words, our understanding of reaction mechanisms for the synthesis of superheavy elements is far from giving suggestions or predictions on a promising experimental way to deal with the superheavy elements. Particularly for *hot fusion*, there are no theoretical frameworks applicable for calculations of formation and survival probabilities. The difficulty is that there is no fusion barrier like in lighter systems, where the fusion probability or fusion cross section is given by a simple formula with the barrier parameters. (We try to discuss in a similar way with the parameter B_{EX} from the view point of dissipative dynamics.) Furthermore, there is no fission barrier for superheavy compound systems at least before the systems cool down enough for restoration of the shell correction energy. In other words, the fission process has to be described with a barrier height which is time dependent due to neutron evaporation, i.e., almost no barrier at the beginning and enough barrier at the end of the process. There is no simple theory or formula to describe such reaction processes. Therefore, it is crucially important to establish a dynamical framework which enables us to calculate final residue cross sections of superheavy nuclides, starting from the contact of two incident heavy ions.

The purpose of the present paper is thus to propose a new dynamical model for synthesis of the superheavy elements from the view point of *hot fusion* or *warm fusion* reaction [32–35], where the theory of Brownian motion [36] is employed to describe the dynamical evolution of the whole fusion and fission process from a contact of two nuclei to a spherical or deformed mononucleus and finally into fission, with an extremely small probability of residues of superheavy nuclei left inside the potential pocket due to the shell correction energy. The model enables us to study two conflicting requirements, larger fusion probability and smaller fission probability, and to find, as a compromise of them, an optimum condition on excitation energy or incident energy of collisions for synthesizing superheavy elements.

As is well known, fusion occurs by overcoming the inner barrier which is located far away from the contact configuration in heavy systems; so we first have to solve dissipative dynamical motions toward the spherical shape as well as toward the reseparations leading to quasifission. It should be noticed here that trajectory calculations with the friction [37–40] have been very useful for the explanation of the extra- or extra-extra-push energy [41–43], but are not suitable for describing extremely small probabilities reaching the spherical shape and around, because in most cases mean trajectories do not reach there and fluctuations around them are indispensable. Therefore, it is necessary to solve a full dissipative dynamics or a fluctuation-dissipation dynamics with the Kramers (Fokker-Planck) equation or with the Langevin equation, taking into account tails of the distribution as well as the mean trajectory.

Of course, there are reactions invoked before reaching the contact, which result in losses of a fraction of incident flux, energy, etc. The losses or a distribution of the losses in the approaching phase are the initial condition for the subsequent dynamics in the composite system which is the object of the present model. So they should be taken into account for precise predictions, but for the moment we assume no loss of probability, energy, etc., considering that they do not essentially change the reaction mechanisms themselves which follow. (Their effects are being investigated and will be published in a forthcoming paper.) As we will see in the following sections, the dynamical processes after contact turn out to diminish the flux or the probability to the spherical shape by several orders of magnitude, i.e., play a decisive role for residue cross sections of superheavy elements. Thus, it is worth studying the dissipative dynamical processes with reasonable initial conditions assumed.

The second important effect we have to take into account carefully is the cooling due to neutron evaporation which comes into play immediately after the composite system is substantially excited with transferred incident kinetic energy and the Q value. As is well known, the cooling restores the shell correction energy which stabilizes the compound nucleus. The crucial point is how fast the potential pocket or the fission barrier appears to keep appreciable probabilities inside before fission is completed. The cooling speed which depends on isotopes, combined with the temperature dependence of the shell correction energy, determines the crucial time dependence of the appearing fission barrier.

As a first step toward the complete dissipative description of fusion-fission processes, we investigate a one-dimensional model with mass symmetry in the present paper. Even in a mass-symmetric system, the fusion and fission paths are different in neck formation, fragments deformation, etc. But their effects could be represented by a slight difference in their one-dimensional potential as a function of deformation or fragment separation. We therefore expect it to be possible to learn the characteristic features of fusion-fission processes and to discuss the optimum condition for the synthesis of the superheavy elements within the one-dimensional model. Furthermore, we assume the overdamped motion just after the contact of two incident ions, considering strong friction like the one-body model to be valid [27,28,44], i.e., the time scale of the momentum thermalization to be far shorter than that of the collective coordinate motion of the fusion-fission process. In the present analyses, we thus employ the Smoluchowski equation [36,45], instead of the Kramers one.

As is inferred from the above simplifications, the present investigation is not for a precise prediction of absolute values of residue cross sections, but for the proposal of the new model which is promising for further developments towards realistic predictions of the way to produce superheavy elements. But as will be given in the following, even with the above drastic simplifications the present model provides a qualitative understanding of the characteristic features of the fusion-fission dynamics in the superheavy mass region. The enhancement of the residue cross sections found at the optimum condition is remarkable. The common sense, that the increase of the excitation energy makes residue cross sections dramatically decrease due to multichance fission [46], is shown to be modified by the strong friction in fissioning motions and by the quick restoration of the shell effect. More realistic calculations including many collective degrees of freedom of the compound systems are being made and will be published in subsequent papers, where various combinations of projectile and target are to be discussed for suggest-

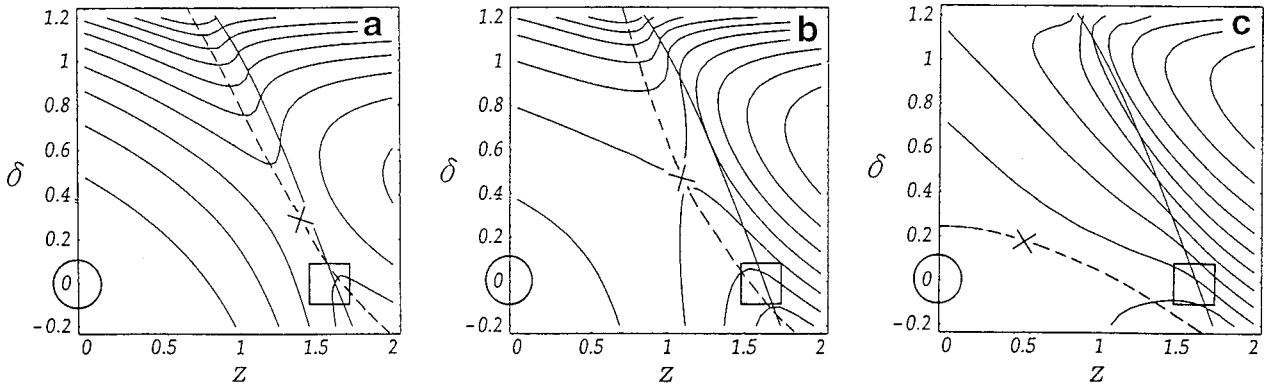

FIG. 1. Macroscopic energy surface in nuclear deformation space. (a) is for $Z=50$, (b) for $Z=80$, and (c) for $Z=114$. The abscissa denotes the separation between two potential centers and the ordinate denotes the fragment deformation. The scission line (zero-neck radius) is denoted by the solid curve and the ridge is given by the dashed line. Symbols are given in the text. The compound nucleus is produced inside the saddle point for the case of $Z=50$ but outside for $Z>80$.

ing promising experiments in the light of the present model.

In the next section, the diffusion model is presented for the analysis of the fusion-fission dynamics. The time dependence of the restoration of the shell correction energy is described with the statistical model in Sec. III. Results of the dynamical calculations are given in Sec. IV, showing how the enhancement of the residue cross sections is obtained as a compromise between the diffusion mechanism and the restoring shell effect, and how it depends on the neutron and proton numbers of the compound nucleus and on the strength of the friction.

Section V is devoted to the discussion on observations of the enhancement, i.e., a relation between the optimum excitation energy and the Bass barrier height. A summary is given in Sec. VI.

II. DIFFUSION MODEL FOR FUSION-FISSION DYNAMICS

The reaction process from the contact of the colliding nuclei to the subsequent reseparation or the formation of compound nuclei leading to evaporation residues is divided into the following two parts: (a) the period from the initial contact to the stage when the dissipation of the relative kinetic energy into the internal one is accomplished and (b), succeeding step (a), the period during which the deformed compound system evolves to the configuration of two separate nuclei or to the compact configuration. In both steps, the time development of the probability distribution is assumed to be governed by the fluctuation-dissipation process on the potential energy surface in a multidimensional shape parameter space, though in step (a) the temperature of the system increases rapidly from zero to the maximum.

When the atomic number of the compound nucleus produced by fusion reaction is less than ~ 70, the configuration of the compound nucleus at the end of step (a) locates inside the unconditional saddle point. Naturally the system at the contact configuration evolves into a compact configuration of compound nucleus with very little probability of reseparation. This means that the fusion probability can be estimated from the information only on the fusion barrier height [47] of the entrance channel where the nuclear interaction starts in action.

In the case that the atomic number of the compound nucleus is around 80–90, the configuration of the system at the end of step (a) critically depends upon the incident energy: i.e., if the incident energy is low, just enough to overcome the incident Coulomb barrier, the system is found outside of the unconditional saddle point. Only when a sufficient extra energy is given is the system found inside the saddle point. The hindrance for fusion that the colliding nuclei cannot fuse with each other without an additional kinetic energy (extra-push energy) [41–43] can be qualitatively explained in the above way.

When the atomic number of the system increases beyond 100, the situation changes dramatically. At the end of step (a), almost all of the configuration will be found at far outside the unconditional saddle point. Therefore, in step (b), the high potential barrier should be overcome in order for the system to fuse into the compact configuration. This is one of the reasons why the extreme decrease of the fusion probability is observed in systems with $Z>100$.

These situations are illustrated in Fig. 1 where the two-center parametrization [48,49] is used for three cases of the atomic number of the compound nucleus $Z=50$, 80, and 114 assuming symmetric deformation (zero mass asymmetry). The solid curves denote the scission line (zero-neck line) which includes an incident touching configuration (marked by squares) and dashed curves denote the ridge passing through the fission saddle point (marked by crosses). Ordinates denote δ (deformation of fragments) and abscissas denote z. The coordinate z is defined as $z=z_0/(R_{CN}B)$, where z_0 and R_{CN} denote the distance between two potential centers and the radius of the spherical compound nucleus, respectively. The parameter B is defined as $B=(3+\delta)/(3-2\delta)$. By this scaling, we can save a great deal of computation time. $z=\delta=0$ corresponds to a spherical compound nucleus (marked by circles). Similar discussions are given also in Ref. [50].

In the present calculations of the evaporation residue cross sections of superheavy nuclei, a drastic assumption is introduced for the process in step (a) without solving the dynamics. At the end of step (a), the probability distribution is assumed to be localized around a point along the fission path where the center-of-mass distance corresponds to that of the touching two spheres which is outside the unconditional

saddle point. That is to say, it is assumed that the relative kinetic energy dissipates just at the touching distance. Though the assumption is a crude approximation for step (a), it is not so inappropriate for studying the fusion process because the time scale of the dissipation is much shorter than that of the collective motion. In this assumption, there is still room for checking the effects of possible variations in the dynamics of step (a) by changing the initial location of the probability distribution. Actually, the dynamics in step (a) is considered to give an initial distribution for the dynamical evolution in step (b). This is being investigated and will be published in a forthcoming paper.

The process in step (b) is described by fluctuation-dissipation dynamics from the initial configuration of a dinuclear system to the formation of the compound nucleus as well as to the reseparation, namely, to the fission back into the symmetric fragments. From the analysis of prescission neutrons and fragment kinetic energies, a strong dissipation comparable to the one-body model is recommended [28], which permits us to use the Smoluchowski equation for fusion-fission dynamics as an approximation of the Kramers or the Langevin equation [29,45].

The Smoluchowski equation is expressed as follows:

$$\frac{\partial}{\partial t}P(x,l;t)=\frac{1}{\mu\beta}\frac{\partial}{\partial x}\left\{\frac{\partial V(x,l;t)}{\partial x}P(x,l;t)\right\}+\frac{T}{\mu\beta}\frac{\partial^2}{\partial x^2}P(x,l;t). \quad (1)$$

$P(x,l;t)$ denotes the probability distribution in the collective coordinate space. The first term on the right hand side of the Smoluchowski equation is the potential term and the second term is the diffusion term. If the potential $V=0$ in the Smoluchowski equation, it is just a simple diffusion equation which is usually called the heat conduction equation with the diffusion coefficient $D=T/\mu\beta$. The coordinate x is defined as $x=R_{\rm c.m.}-\frac{3}{4}r_0A^{1/3}$ so that $x=0$ corresponds to the spherical shape, where $R_{\rm c.m.}$ denotes the separation distance between the mass centers of two incident nuclei or the nascent fission fragments, A the mass number of the nucleus, and $r_0=1.16$ fm. The angular momentum of the system is expressed by l. Both the inertia mass μ and the reduced friction β are assumed to be independent of the shape of nucleus in the present calculations. The parameter μ is taken to be the reduced mass for the symmetric separation and β is taken to be 5×10^{21} s^{-1} [45] which is consistent with the value of the one-body dissipation in a series of shapes. Note that Eq. (1) actually does not depend on the inertia mass, but only on the friction $\gamma=\mu\beta$.

The potential $V(x,l;t)$ is composed of the energy of the droplet model and of the shell and the pairing correction energy whose details will be described in the next section. Here, it is mentioned that $V(x,l;t)$ is a function of x, l, and t. The time dependence enters through the time dependence of the temperature T of the system. The potential $l=0$ and with and without the shell correction energy is shown in Fig. 2 for the nucleus with $Z=114$ and $N=184$.

The initial probability distribution $P(x,l;t=0)$ is taken to have a Gaussian shape with a very small width and is imposed at around $x_0=x_{\rm cont}-0.5$ fm, where $x_{\rm cont}$ is the contact

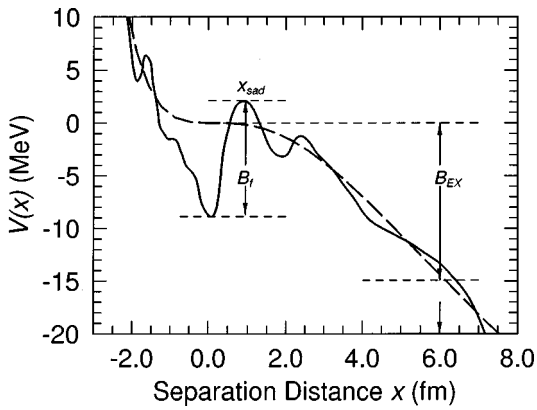

FIG. 2. The finite-range droplet model energy for the element 114 is drawn by the dashed line and the potential energy including the shell and pairing corrections by the solid line. The abscissa denotes x (separation distance between the mass of two nascent fragments). The initial probability distribution is settled at the point x_0, which is marked by the arrow. The fission barrier with shell corrections B_f and the difference $B_{EX}=V_{\rm DM}(x_{\rm sad})-V_{\rm DM}(x_0)$ are illustrated.

distance evaluated as $x_{\rm cont}=2r_0(A/2)^{1/3}-\frac{3}{4}r_0A^{1/3}$. The position of x_0 is marked by the arrow in Fig. 2 for $A=298$. In Fig. 2, the fission barrier height with the shell correction energy is denoted by B_f, and the difference between the droplet model energy at the first saddle point $x_{\rm sad}$ and that at the initial point x_0 is denoted by B_{EX}. As will be discussed in the next section, B_{EX} is a very important quantity in the formation process because it is, so to speak, the fusion barrier height that the system has to overcome by diffusion in order to reach the compact configuration.

Here, we define the compound-nucleus (CN) probability $d(T_0,l;t)$ that the system is inside the saddle point $x_{\rm sad}$:

$$d(T_0,l;t)=\int_{-\infty}^{x_{\rm sad}}P(x,l;t)dx, \quad (2)$$

where T_0 is the initial temperature to be calculated from the incident kinetic energy and the reaction Q value. At the beginning instance of the fusion process ($t=0$), all of the probability $P(x,l;t=0)$ is located around the initial point x_0: therefore $d(T_0,l;t=0)=0$, and then the probability d increases because a part of probability $P(x,l;t)$ climbs up the fusion barrier height B_{EX} and comes inside the saddle by diffusion. At the early stage of the time evolution, probability d is considered to be the time-dependent formation probability. Then the probability accumulated in the left inside the saddle point $x_{\rm sad}$ diffuses back over the fission saddle point and goes down the potential slope; consequently a decrease of the probability d occurs. At the final stage of the cooling process, due to the restoration of the shell correction energy, a part of the incident flux, though it is very small, is kept around the compact configuration. The probability d at $t\rightarrow\infty$ describes the evaporation residue probability.

Using the probability d, the evaporation residue cross section $\sigma_{\rm EV}$ is calculated as

$$\sigma_{EV}=\frac{\pi\hbar^2}{2\mu_0E_{\rm c.m.}}\sum_l(2l+1)d(T_0,l;t=\infty), \quad (3)$$

where μ_0 denotes the reduced mass in the entrance channel and $E_{\text{c.m.}}$ the incident energy in the center-of-mass frame.

III. TEMPERATURE-DEPENDENT POTENTIAL ENERGY SURFACE

The time-dependent potential energy appearing in Eq. (1) is defined as follows:

$$V(x,l;t)=V_{\text{DM}}(x;t)+\frac{\hbar^2 l(l+1)}{2I(x)}+V_{\text{shell}}(x)\Phi(t),$$

$$V_{\text{DM}}(x;t)=[1-\xi T^2(t)]E_S(x)+E_C(x), \tag{4}$$

where $I(x)$ is the moment of inertia of a rigid body at deformation x. Here V_{shell} is the shell plus pairing correction energy at $T=0$, and V_{DM} is the potential energy of the finite range droplet model at time t, i.e., at temperature $T(t)$. Here E_S denotes the sum of the surface and the curvature energy, and E_C is the Coulomb energy of the droplet model. These are calculated with the code developed by Möller *et al.* [5]. The temperature-dependent factor for E_S is introduced with $\xi=0.014$ MeV^{-2} [51]. The potential energy curve along the fission path is calculated with the ϵ parametrization [52] and is shown in Fig. 2 for the nucleus with $Z=114$ and $N=184$ as described in the previous section. The solid and dashed curves denote $V_{\text{DM}}+V_{\text{shell}}$ and V_{DM} alone, respectively. When the nucleus is at high temperature, the shell plus pairing correction energy disappears. It however restores as the nucleus cools down, and the potential energy curve changes gradually from the dashed curve to the solid one. Thus, one of the most important ingredients is the shell and the pairing correction energies depending on the shape and temperature of the composite system.

The temperature dependence of the shell correction energy expressed by $\Phi(t)$ in Eq. (4) is extracted from the free energy [53] calculated with single-particle energies [54],

$$F(T)=\sum_i \epsilon_i f(\epsilon_i,T)-T\Bigg\{-\sum_i [f(\epsilon_i,T)\ln f(\epsilon_i,T) + \overline{f}(\epsilon_i,T)\ln \overline{f}(\epsilon_i,T)]\Bigg\}, \tag{5}$$

where ϵ_i is the energy of the ith single-particle level, $f(\epsilon_i,T)$ the Fermi distribution function at temperature T, and $\overline{f}(\epsilon_i,T)=1-f(\epsilon_i,T)$. The details are given in Appendix A.

We assume that both the shell and the pairing correction energies have the same dependence on temperature; hereafter, the term ''shell correction energy'' is used to refer to the shell plus pairing correction energy. The calculated free energy is found to be consistent with the parametrization of the factor $\Phi(t)$,

$$\Phi(t)=\exp\left(-\frac{aT^2(t)}{E_d}\right), \tag{6}$$

following the work by Ignatyuk *et al.* [55], where a denotes the level density parameter of Töke and Swiatecki [56]. The shell-damping energy E_d is chosen as 20 MeV according to our results, which is consistent with that given by Ignatyuk *et al.* [55]. The cooling curve $T(t)$ is calculated by the statistical model code SIMDEC [54]. The details about SIMDEC are given in Appendix B.

As for the damping of shell effects, there is seemingly a discrepancy between the microscopic calculations and the experiments which indicate almost no shell stabilizing effect of the $N=126$ neutron shell. In order to understand the strong damping of the shell effects, the collective enhancement of the level density, the temperature-induced deformation, etc., have been investigated, but up to now a definite conclusion has not been reached; nor is it yet clear whether the seemingly strong damping is general, not specific, to $N=126$ [30]. Thus, we adopt the calculated result for the damping energy E_d ($\sim$20 MeV) in the following calculations.

IV. NUMERICAL RESULTS

A. Excitation function of evaporation residue cross section for $Z=114$

Now it is in order that we present the residue excitation function calculated by the present dynamical model, taking as an example the reaction forming the superheavy nucleus with the doubly closed shell, i.e., the reaction $^{149}_{57}\text{La}+^{149}_{57}\text{La}\rightarrow{}^{298}114$. For the purpose of understanding well the characteristic enhancement in the excitation function which we will see below, we first discuss the CN probability of one partial wave, i.e., of $l=10$, which is one of the dominantly contributing partial waves. As is given in Eq. (2), the CN probability d is a function of time, which is described by the diffusion equation (1). As is stated in Sec. II, the physical probability responsible for the observed cross section is that at time t equal to infinity.

Figure 3(a) shows the time dependence of $d(T_0,l=10;t)$ for five different initial temperatures $T_0=0.68$, 0.79, 0.96, 1.11, and 1.24 MeV, which, of course, correspond to five different excitation energies $E^*=15.0$, 20.0, 30.0, 40.0, and 50.0 MeV, respectively, and hence to five different incident energies. They all increase in the beginning and later on start to decrease or stay almost constant, which is easily understood by the diffusion picture. Up to the time around 10×10^{-21} s, the probability in the region of the compact configuration is supplied by diffusion from the contact region and its yield increases rapidly. The higher the temperature T_0 is, the larger the diffusion into the compact configuration is obtained, so the larger probabilities at the beginning. But during that time, the main part of the probability initially around x_0 descends down the slope of the potential and thus meanwhile the supply ceases. After $t\sim10\times10^{-21}$ s, the probability accumulated in the compact configuration area diffuses back over the fission barrier arising from the restoration of the shell correction energy. At a low temperature such as $T_0=0.68$ MeV, 47% of the shell correction energy is restored already and the fission barrier is about 5 MeV. Therefore, the fission width becomes very small and $d(T_0,l;t)$ approaches its final value quickly and stays almost constant. On the contrary, in the case of $T_0=1.24$ MeV, only 10% of the shell correction energy is restored and the fission barrier is about 1 MeV. The restoration takes about

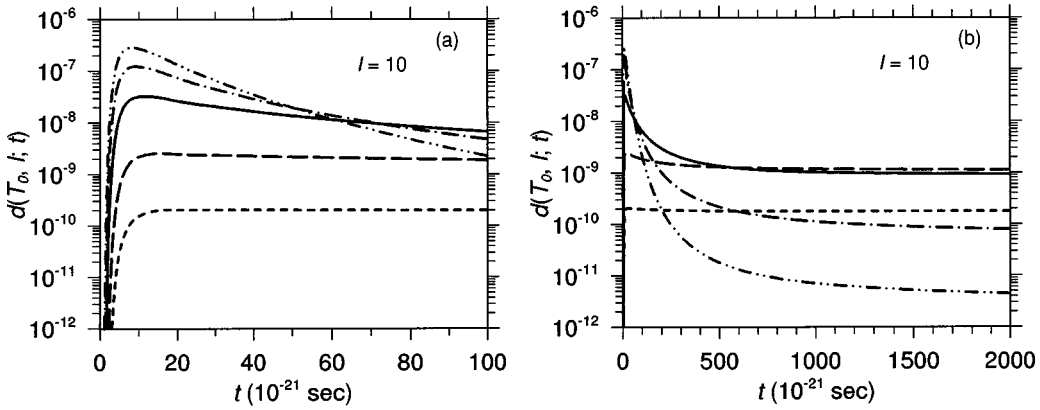

FIG. 3. (a) The time evolution of the CN probability $d(T_0,l=10;t)$. The curves for five initial temperatures are plotted: $T_0=0.68$ (short-dashed line), 0.79 (long-dashed line), 0.96 (solid line), 1.11 (dot-dashed line), and 1.24 (double-dot-dashed line) MeV. (b) Their long-time behaviors are shown.

500×10^{-21} s to become enough to prevent the system from fissioning (at this time, $T=0.76$ MeV and the restored fission barrier is about 4 MeV) and during the time the yield accumulated in the compact configuration area diffuses out rapidly, which gives the dramatic decrease shown in Fig. 3(a).

It is interesting to see their long-time behaviors which are shown in Fig. 3(b) and which we now plot up to $t=2000\times10^{-21}$ s. In the competition between the neutron evaporation and the fission, the neutron evaporation width Γ_n is expressed by using the Weisskopf model [57]:

$$\Gamma_n=\frac{gm}{\pi^2\hbar^2}\frac{1}{\rho(E^*)}\int d\varepsilon\,\sigma_{\rm abs}(E',\varepsilon)\varepsilon\rho_D(E')\propto\exp(-B_n/T), \tag{7}$$

where B_n denotes the neutron separation energy. The fission decay width Γ_f can be estimated from the quasistationary solution of the Smoluchowski equation (1) as

$$\Gamma_f=\frac{\hbar\omega_0\omega_s}{2\pi\beta}\exp(-B_f/T), \tag{8}$$

where ω_0 and ω_s are the oscillator frequencies of the two parabolas approximating to the potential $V(x)$ in the first minimum at $x=x_0$ and at the saddle point $x=x_s$, respectively [58]. Note that the essential factor $\exp(-B_f/T)$ is common with the Bohr-Wheeler model [59]. At $t\sim2000\times10^{-21}$ s in this system, B_f is almost equal to B_n, which is about 5 MeV. Therefore, we find that Γ_f is comparable with Γ_n:

$$\frac{\Gamma_n}{\Gamma_n+\Gamma_f}\sim\frac{1}{2}. \tag{9}$$

To save computation time, we regard the time $t=2000\times10^{-21}$ s as t_∞, which might cause an error of a factor of 2 in the absolute values.

The cases with larger probabilities at the beginning do not always stay so at later time. Actually the case with $T_0=1.24$ MeV, for example, is seen to go down to the next to the smallest at the final time. The higher initial temperatures require longer time for the system to cool down enough for the restoration of the fission barrier, during which most probabilities diffuse back to fission. This is the reason why scientists think seriously about so-called *cold fusion* instead of *hot fusion*. But this fact, combined with the fact that the case with the lowest initial temperature results in the smallest fusion probability due to the small diffusion into the compact configuration at the beginning, leads to the existence of the optimum initial temperature, being neither so low nor so high. This is clearly seen in Fig. 4 where the solid line connecting the open triangles denotes the CN probability at $t=2000\times10^{-21}$ s as a function of excitation energy, showing the maximum around $E^*=25$ MeV.

Because of the difference in time scale between formation and decay as is readily seen in Fig. 3(b), the characteristic

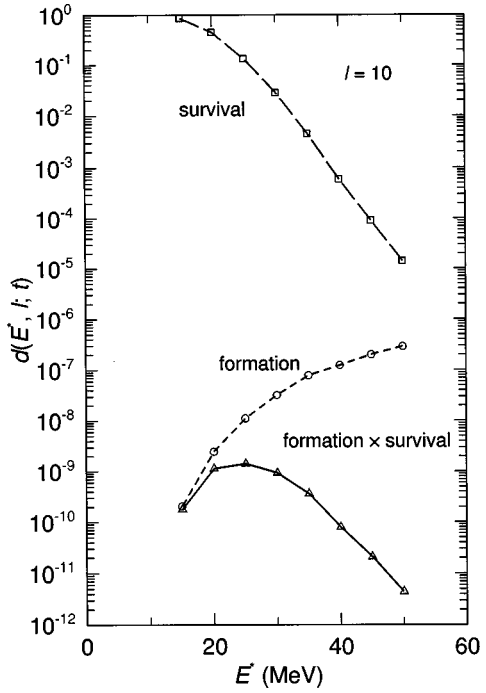

FIG. 4. The peak value of $d(T_0,l;t)$ in Fig. 3(a) corresponding to the ''formation'' probability (open circles connected by the short-dashed line) and the ratio of the peak value and the stationary value at $t=2000\times10^{-21}$ s corresponding to the ''survival'' probability (open squares connected by the long-dashed line) are shown. The product of the above two factors is drawn by open triangles.

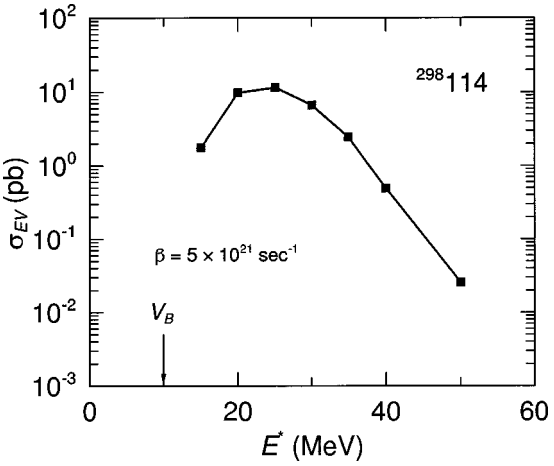

FIG. 5. The excitation function of the evaporation residue cross section for the $^{149}_{57}$La+$^{149}_{57}$La$\rightarrow^{298}$114 reaction calculated from $d(T_0,l;t_\infty)$. The value of the reduced friction parameter β is set to 5.0×10^{21} s^{-1}.

energy dependence of the final residue probability can be understood by decomposing themselves into two factors: ''formation'' probability and ''survival'' probability. The height of the peak around 10×10^{-21} s is essentially determined by the diffusibility into the compact configuration area and is plotted by open circles in Fig. 4 which represent ''formation'' probabilities. The decrease from the peak value to the final yield at $t_\infty=2000\times10^{-21}$ s depends on how fast the fission barrier grows enough by the restoration of the shell correction energy. The ratios of the peak value to the final yield are plotted in Fig. 4 by open squares, which represent ''survival'' probabilities. The former is simply controlled by a diffusion mechanism on the potential energy surface with the diffusion coefficient T/γ and thereby increases as the excitation energy (temperature) increases, while the latter is controlled by diffusion over the restoring, i.e., time-dependent, fission barrier due to the cooling, and thereby decreases as the excitation energy increases. It should be emphasized here that the ''formation'' and the ''survival'' probabilities are dynamical quantities, not those which are described by the barrier penetration and by the statistical decay.

Then, we calculate the excitation function of fusion residue cross section by summing up all the partial waves according to Eq. (3), which is shown in Fig. 5. A similar enhancement to the case of $l=10$ shown in Fig. 4 is seen in the cross section $\sigma_{\rm EV}$ around $E^*=25$ MeV; i.e., the optimum excitation energy exists for synthesizing the superheavy element. As discussed above, this is due to the two competing factors having opposite energy dependence, ''formation'' and ''survival'' probabilities, not due to the usual origin of the maximum fusion cross section, i.e., an accumulation of partial wave as the incident energy increases and a disappearance of the fission barrier at a certain high angular momentum. Therefore, the present mechanism for the optimum energy is completely new and unexpected. Of course it does not always happen that the two factors generate the bell-shaped enhancement as shown above. As stated in the Introduction, the crucial point is how quick the cooling due to evaporation is or how slow the fissioning motion is. The former is essentially determined by the speed of the neutron evaporation.

Since the neutron decay probability is proportional to $\exp(-B_n/T)$, the smaller the separation energy B_n is, the quicker the cooling speed is. Therefore, whether the optimum energy exists or not depends on the isotopes, which is investigated in Sec. IV B. The latter is controlled by the strength of the friction force which results in the reduction of the factor $1/\beta$ in the fission decay width.

At the same time, it affects also the time scale of diffusion into the compact configuration, i.e., ''formation'' probability. This is discussed in Sec. IV C. Of course, absolute values of shell correction energies of the ground states of various compound nuclei are basically important quantities, which depend on proton number Z as well as neutron number N. The Z dependence is the subjects of Sec. IV D. Before proceeding to these subjects, we briefly discuss the possible ambiguities: the initial condition of the calculations and the level density parameter.

The peak values in Figs. 3(a) and 3(b), i.e., the ''formation'' probabilities, depend on the initial position x_0, which are taken to be close to the touching point of the two spheres of the incident nuclei. There the relative kinetic energy is assumed to be transferred into internal thermal energy. If we take into account a deformation of the incident nuclei, x_0 would be larger. The increase of x_0 by 1 fm makes the starting point lower by about 3 MeV in the potential energy, which means that the system has to climb up by diffusion by about 3 MeV more in order to reach the compact configuration. This results in a decrease of the ''formation'' probability by about one order of magnitude and, accordingly, in the reduction of the optimum cross section. Realistic values of x_0 or realistic distributions of x_0 due to the dynamics before the total incident kinetic energy damps completely will be investigated by the Langevin equation and their effects on final residue cross sections will be discussed in the forthcoming paper. Anyhow, the initial momentum pushes the system toward the inside and thus is expected to increase the ''formation'' probabilities.

Another ambiguity is the level density parameter a which governs the statistical decays and thus affects the speed of the cooling. Since the parameter a itself depends on temperature, we here investigate the effects of its temperature dependence on the cooling. Figure 6 shows the cooling of the compound nucleus with $Z=114$, $N=184$, and the initial excitation $E^*=30$ MeV. The solid and dashed curves correspond to the cases using the constant and temperature-dependent level densities [55], respectively. The two curves cross each other, which can be understood from the decay width for neutron emission. As a whole, it is found that the calculated value of the residue cross section does not change so much by the introduction of the T-dependent level density parameter. Therefore, we use the constant level density in the present calculations.

B. Isotope dependence of the evaporation residue cross section

Naively speaking, neutron-rich isotopes are considered to give rise to a large residue cross section, because they generally have large neutron decay widths and thereby are fa-

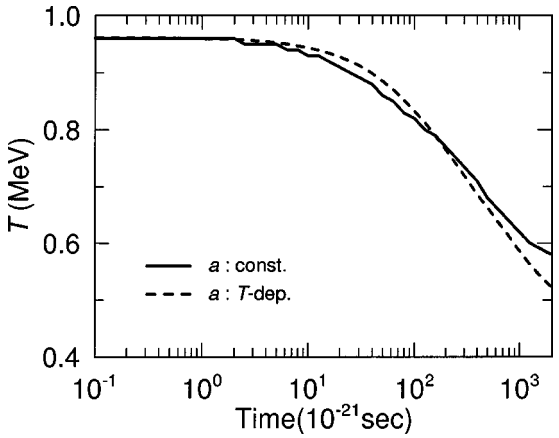

FIG. 6. The cooling curve for the initial temperature $T_0 = 0.96$ MeV. Two cases are compared: the temperature-dependent level density parameter (dashed line) and the constant value (solid line).

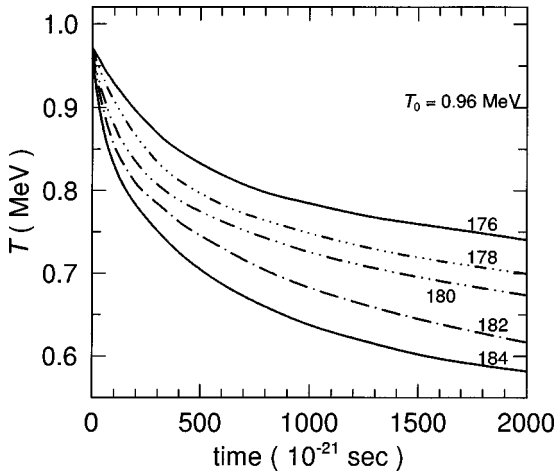

FIG. 8. The isotope dependence of the cooling curve for $Z = 114$ with the initial temperature $T_0 = 0.96$ MeV. Figures denote neutron numbers.

vored in the survival probability Γ_n/Γ_f. However, the neutron richness has an additional meaning in the present dynamical model. As discussed in the previous subsection, the cooling due to neutron evaporation restores the shell correction energy which prevents fission. Consequently, the fission decay widths Γ_f become smaller due not only to the time dependence of temperature but also to the time dependence of the appearing fission barrier. Therefore, in the present model neutron-rich isotopes are expected to be favorable for larger residue cross sections due not only to large neutron decay widths but also to small fission decay widths.

Figure 7 shows the results of the calculations for a series of $Z = 114$ isotopes with $N = 176$, 178, 180, 182, and 184. Here we always take symmetric incident channels with ^{145,146,147,148,149}La nuclei. Actually, the favorableness of neutron-rich isotopes, as we discussed above, is clearly seen in Fig. 7. And the optimum position shifts to higher energy in the neutron-rich isotopes, while in the neutron-deficient isotopes the enhancements attenuate, and even disappear, for

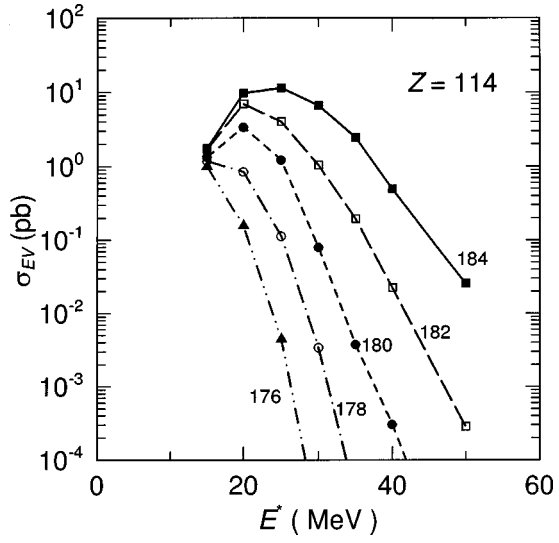

FIG. 7. The isotope dependence of the excitation function of the evaporation residue cross section for $Z = 114$. Figures denote neutron numbers.

$N = 176$ and 178. In such isotopes, we have to go as low in energy as possible, i.e., to so-called *cold fusion*, which is consistent with the experiences of GSI [14,20].

Now we explain the isotope dependence of the evaporation residue cross sections by using the cooling curves. In order to see how sensitive the cooling speed is to neutron number N, we calculate the time dependence of the temperature for $N = 176$, 178, 180, 182, and 184 with the starting temperature $T_0 = 0.96$ MeV ($E^* = 30$ MeV), which is shown in Fig. 8. At this temperature, the fission barrier height is about 2 MeV with which the fission decay of the compound nucleus is possible with a considerable probability. When the temperature cools down to 0.76 MeV ($E^* = 20$ MeV), which corresponds to the shell dumping energy E_d in Eq. (4), 36% of the shell correction energy is restored and the fission barrier height becomes about 4 MeV, which is enough to prevent the fission decay of the compound nucleus in the spherical region. Therefore, the duration t_a for cooling from $T_0 = 0.96$ MeV to $T_a = 0.76$ MeV is an important index which represents the cooling speed. Apparently, there are large differences in the time dependence, which results in surprising differences of the restoration of the shell correction energy, and hence in differences of fission decay width or life.

In the case of $N = 184$, the characteristic time t_a is very short such as 250×10^{-21} s. Therefore, most of the probability accumulated in the spherical region survives against fission, due to the quick restoration of the shell correction energy. On the contrary, in the case of $N = 176$, t_a is long such as 1500×10^{-21} s. During this time most of the compound nuclei in the spherical region decay by fission. The evaporation residue cross section depends on t_a and the increase in t_a by 200×10^{-21} s makes a decrease of the evaporation residue cross section by about one order of magnitude.

It would be meaningful to discuss the relation of neutron binding energy to the cooling speed. Since the energy release by one neutron emission is approximately equal to $2T + B_n$, we might think that cases with large B_n, i.e., neutron-deficient isotopes, are quick in cooling. But the cooling speed is proportional to the product of the amount of the energy removed by one emission and the emission rate,

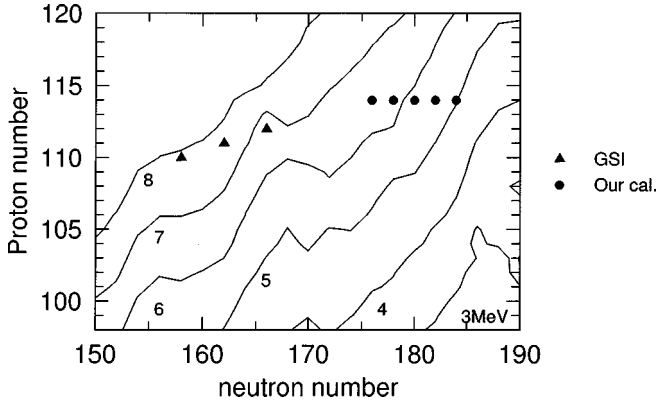

FIG. 9. A contour map of the neutron separation energy averaged over four successive neutron emissions $\langle B_n \rangle$. The numerical numbers associated with lines are $\langle B_n \rangle$ values in MeV. Three triangles indicate isotopes which GSI succeeded in synthesizing by *cold fusion*. The solid circles indicate those which are investigated in the present paper.

$$-\frac{dE}{dt} = (2T + B_n)\frac{\Gamma_n}{\hbar} \tag{10}$$

or

$$\frac{dT}{dt} = -\frac{2T + B_n}{2aT}\frac{\Gamma_n}{\hbar} \propto (2T^2 + B_n T)\exp(-B_n/T). \tag{11}$$

Because of the dominant exponential factor, the cooling speed is higher for smaller B_n and hence for neutron-rich isotopes. Therefore, separation energies B_n over relevant isotopes are very important for the synthesis of superheavy elements in addition to the shell correction energy.

In Fig. 9, a contour map of the neutron separation energy averaged over four successive neutron emissions $\langle B_n \rangle$ is displayed calculated from Möller's mass table [5]. The numerical numbers associated with lines are $\langle B_n \rangle$ values in MeV. Naturally neutron-rich isotopes have smaller $\langle B_n \rangle$'s than those of neutron-deficient ones. Three triangles indicate isotopes which GSI succeeded in synthesizing by *cold fusion* [14,20]. Their $\langle B_n \rangle$'s are 7–8 MeV; so there is no hope for the quick cooling necessary for the enhancement in higher energies, which is consistent with GSI experiments. On the other hand, the dots indicate those which are investigated in the present paper with $\langle B_n \rangle$'s equal to 5–6 MeV, where some of them show the enhancement. It is expected that even more neutron-rich isotopes are more favorable for the enhancement of residue cross sections. Thus, an exploration of the experimental feasibility of reaching the neutron-rich side of the superheavy elements is an extremely interesting and urgent subject. More detailed studies of the isotope and isotone dependence will be given in forthcoming paper.

C. Friction parameter dependence

Since the strength of the friction is not well determined yet, and even its order of magnitude is under debate [29], it is necessary to know how its variation affects the excitation function of the evaporation residue cross section, which is also useful for understanding the role of friction in the reaction process. In the present work, the value of the friction parameter β appearing in the Smoluchowski equation is taken to be 5.0×10^{21} s^{-1}, which is comparable to the smallest value among the variation of the one-body wall-and-window friction which depends on the deformation.

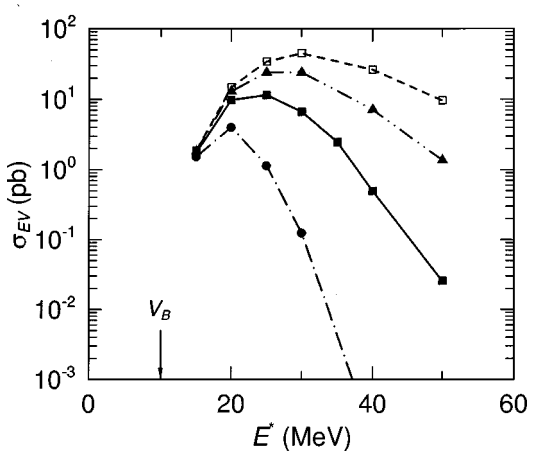

FIG. 10. Dependence of the evaporation residue cross section on the strength of the friction. Results for four values of reduced friction parameter β are plotted: $\beta = 2.5\times10^{21}$ s^{-1} (solid circles), 5.0×10^{21} s^{-1} (solid squares), 7.5×10^{21} s^{-1} (solid triangles), and 10.0×10^{21} s^{-1} (open squares).

The results for $\beta = 2.5, 5.0, 7.5, 10.0\times10^{21}$ s^{-1} are given in Fig. 10. In general, for larger values of β, the cross section is enhanced due to the increase of the survival probability of spherical-like nuclei kept inside the fission barrier. The position of the optimum cross section shifts to higher excitation energies as the friction becomes stronger. As can be seen from the figure, no prominent optimum is expected to appear for small values of β less than 2.5×10^{21} s^{-1}.

Since the friction parameter β appears in the denominator of the right-hand side of the Smoluchowski equation (1), it has a close relation with the time scale of the diffusion process. Thus, the change in the value of β gives rise to a similar effect given by the change in the cooling time due to neutron evaporation. If the value of β increases by twice, the diffusion process governed by the Smoluchowski equation proceeds slowly also by twice and in consequence it is equivalent to a virtual acceleration of the cooling process. This results in a relatively rapid restoration of the fission barrier by the shell correction energy and brings about the enhancement of the survival probability or of the residue cross section. In the reverse case, the virtual cooling speed becomes slower and the fission decay probability relatively increases because of the relative delay of the restoration of shell effects. Briefly speaking, quick cooling or neutron richness has the same tendency as that of strong friction concerning the enhancement of the residue cross section in the higher energies.

In the initial stage of the formation process, the effects of friction are expected to be important and will be given in the forthcoming paper including the effect of the damping of the initial kinetic energy.

D. Systematic calculations around $Z = 114$

It is interesting to see how the excitation function for the evaporation residue cross section depends on Z number. The

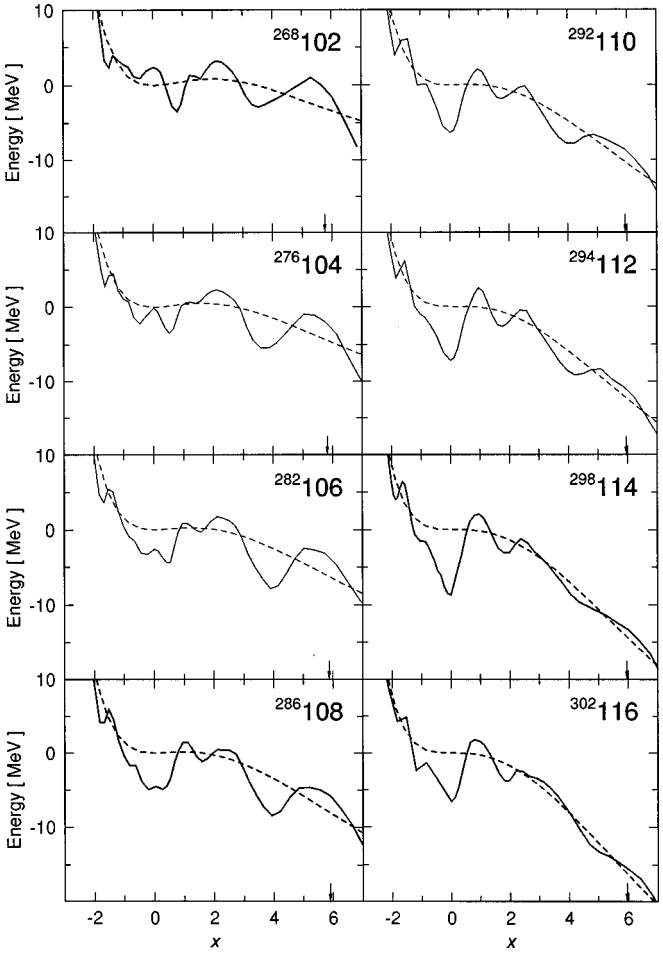

FIG. 11. The potential energy curves along the symmetric fission path for various systems from $Z=102$ to 116 are shown. The solid curve and the dashed curve are the potential energy with and without the shell correction energy, respectively. The initial probability distributions are settled at the points x_0, which are marked by the arrows.

change of the Z number gives rise to the corresponding variation in the potential energy surface due to the change of fissility. The potential energy is represented by V_{DM} and V_{shell} in Eq. (4). The change of V_{DM} influences the ''formation'' probability, while the change of V_{shell} influences the ''survival'' probability, which we will see below.

The cooling of a compound nucleus is essentially determined by the separation energies of neutrons. Therefore, in order to see clearly the Z number dependence of the evaporation residue cross section, the neutron number of compound nuclei for different Z is so determined that the time scale of cooling is the same. The neutron numbers of the initial compound nuclei (Z,N) are thus chosen to be (102, 166), (104, 172), (106, 176), (108, 178), (110, 180), (112, 182), (114, 184), and (116, 186), where the average neutron separation energies are about 5 MeV. (They correspond to the nuclides on the contour line of 5 MeV in Fig. 9.) The same time scale of cooling means that the time scale of the restoration of the shell correction energy is the same. In this way, we can see exclusively the Z number dependence of the cross section, in particular the effects of the absolute value of the shell correction energy in different Z (and N).

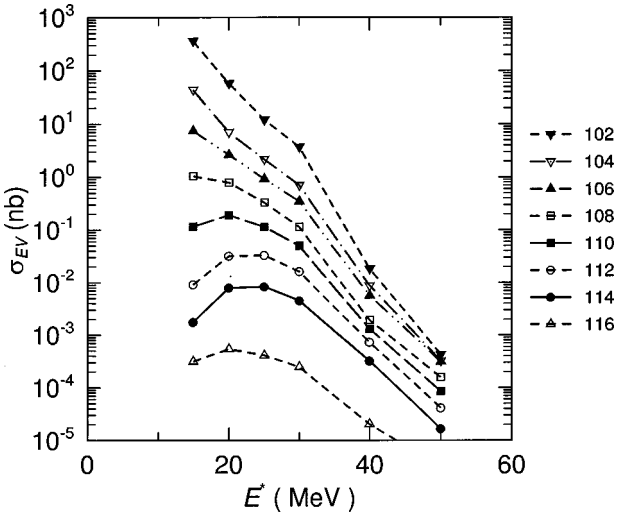

FIG. 12. The excitation function of the evaporation residue cross section that forms the compound nucleus from $Z=102$ to $Z=116$ through the symmetric entrance channel.

In this mass region, the macroscopic fission barrier height estimated from the finite-range droplet model is very small, less than 1 MeV. However, the shell correction energy which works effectively for stabilizing the nucleus against fission varies from 6 MeV to 11 MeV as is shown in Fig. 11 by the solid line. We can see that the nuclei around $Z=114$ and $N=184$ have a large shell correction energy, while it is small for nuclei far from there.

Figure 12 shows the excitation functions of residue cross sections for the above compound nuclear systems, for which we always take symmetric incident channels. In Fig. 12, we can see the characteristic enhancement of the residue cross section at $E^*\sim 25$ MeV in the systems around $Z=114$. In the systems with $Z=102-108$, although the speed of cooling is same for all systems, the enhancement is not seen. We can see the enhancement only in the systems which have a large shell correction energy.

In order to have a clear understanding of the feature of the Z dependence shown in Fig. 12, we focus our attention on the two factors, i.e., the ''formation'' and the ''survival'' probabilities. The former is the probability that the system overcomes the extra potential barrier from the contact point to the spherical configuration area (see Fig. 2) and can be expressed roughly by $\exp(-B_{EX}/T)$. The latter is the ''survival'' probability against fission for the system once diffused into the spherical configuration area and can be expressed by $\exp(-B_f/T)$ approximately. The variations of B_{EX} and B_f with atomic number are shown in Fig. 13. The values of B_{EX} stem from the LDM potential energy, and B_f is the fission barrier height including the shell correction energy. From Fig. 13, we can understand that the monotonous decrease of the yield of residue cross sections with the increase of Z shown in Fig. 12 is due to the monotonous increase of the extra potential barrier height B_{EX} as a function of Z, and that the enhancement of the yield of the residue cross sections around $Z=114$ and $N=184$ is from the strong shell correction energy in the corresponding systems ensuring the large fission barrier height.

Even if there is the enhancement of the evaporation residue cross section, it seems very difficult to synthesize nuclei

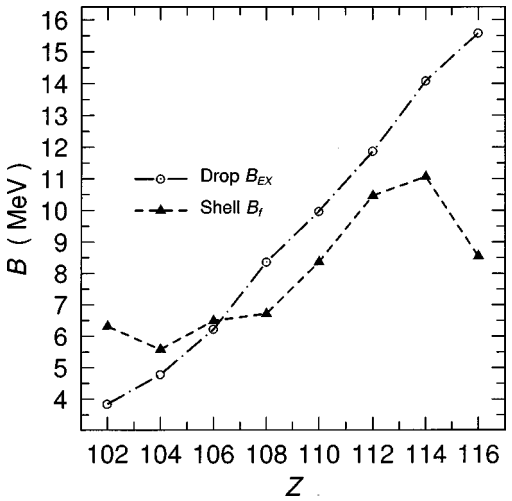

FIG. 13. The ground state fission barrier height B_f and the potential difference B_{EX} defined in Fig. 2. The constant increase of B_{EX} with Z reduces the fusion probability exponentially. The increase of B_f toward $Z=114$ makes an enhancement of the residue cross section as shown in Fig. 12, even though the fusion probability decreases to $\sim 10^{-8}$.

with $Z \geqslant 116$ with detectable probability because the ''formation'' probability decreases with increasing Z number due to the large value of B_{EX}. We thus expect to synthesize superheavy nuclei around $Z=114$ and $N=184$ which have a large shell correction energy and small neutron separation energy $\langle B_n \rangle$.

V. OPTIMUM EXCITATION ENERGY AND BASS BARRIER HEIGHT

The positions of the optimum excitation energy that we have discussed are bounded on the high excitation energy side by the decay properties of compound systems, i.e., by the competition between fission and neutron evaporation. If they are lower than the threshold energy of an incident channel that we choose, we cannot observe the enhancement experimentally. In order to observe or utilize the enhancement, we thus have to choose an incident channel so that the excitation energy of the compound nucleus formed at the incident energy corresponding to the Bass barrier height should be lower than the optimum energy. Otherwise, the system of the incident channel has to undertake so-called subbarrier fusion to hit the optimum energy, and then suffers from a drastic reduction and a strong energy dependence, and thereby the bell shape of the enhancement could not be discernible.

In the present case of the mass-symmetric incident channel, the Bass barrier height is 325 MeV in the center-of-mass system, which corresponds to the excitation of the compound system $E^*=10$ MeV as shown by an arrow in Fig. 5. Therefore, it is meaningful to discuss the excitation function of the reaction, the bell-shape enhancement of which is expected to be observed experimentally if the target and the beam were available. In the following, we denote the excitation energy corresponding to the Bass barrier height by $E^*_{\rm Bass}$.

Generally, the relative position of $E^*_{\rm Bass}$ and the optimum excitation energy depends on combinations of target and projectile. The energy $E^*_{\rm Bass}$ varies almost linearly with respect

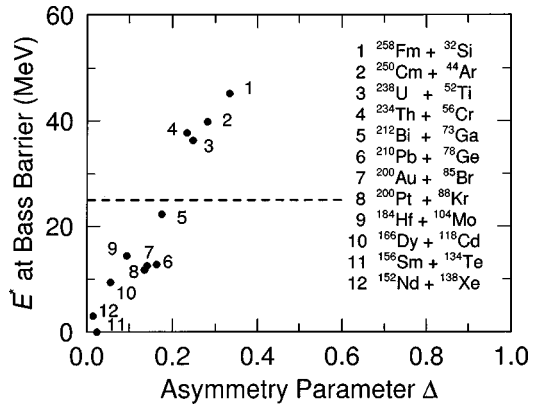

FIG. 14. The excitation energy at the Bass barrier energy $E^*_{\rm Bass}$ is plotted against the mass asymmetry parameter Δ for several combinations of target and projectile that produce the element 114. The dashed line denotes the optimum excitation energy corresponding to the maximum cross section in our present calculation for $N=184$.

to the asymmetry parameter Δ [41] of the entrance channel. This is shown in Fig. 14 for the compound nucleus with $Z=114$ and $N=170-180$, and is compared with the optimum excitation energy corresponding to the maximum cross section in our model calculation, indicated by the dashed horizontal line. There, we see that the observation of the optimum cross sections is possible in systems below the dashed line, where the optimum excitation energy is above $E^*_{\rm Bass}$. Of course the mass asymmetry degree of freedom is expected to change the fusion probabilities quantitatively, which is now being investigated and will be given in the forthcoming paper.

VI. SUMMARY

A long-standing subject of synthesizing superheavy elements is theoretically challenged with the fluctuation-dissipation dynamics which describes the whole process of the collective motions from the contact of the incident heavy ions to the evaporation residues, with most probabilities going back into fission. To our knowledge, this is the first attempt for dynamical calculations of the synthesis of superheavy elements.

Assuming that nucleonic degrees of freedom are in thermal equilibrium immediately after contact of the ions and that the frictional force is strong enough for the collective degree of freedom to be described as an overdamped motion, we employ Smoluchowski equation for fusion-fission and fusion evaporation residue formation processes. In order to show clearly the reaction mechanism, we take a mass-symmetric incident channel and use a simplified one-dimensional model for fusion and fission processes, though we know that there is a difference between fusion and fission paths which would not give a crucial effect. (Actually we have studied the reaction in the two-dimensional model where the difference is taken into account. The results, which validate the assumption, are obtained and will be given in a forthcoming paper.)

The time evolution of the probability distribution of the compound nucleus with $Z=114$ and $N=184$ is solved as an

example using the friction strength $\beta=5\times10^{21}$ s^{-1} and the shell correction energy calculated with the single-particle spectrum of the Woods-Saxon potential. It is found that there exists an optimum excitation energy of the compound nucleus to be initially formed. This is surprising and appears contradictory to our experiences that fission exclusively dominates to leave nothing for residues in higher excitations, but turns out to be consistent and realistic after careful investigations of possible variation of physical parameters.

The optimum energy is a compromise of two conflicting requirements for maximizing final residue cross sections. Since without the shell correction energy there is no potential pocket in the energy surface, the speed of the restoration of the shell correction energy, i.e., the cooling speed, is crucial for the probability to be captured inside the emerging barrier which gives residues of the superheavy nuclides. In other words, in order to obtain large residue cross sections the cooling should be quick or the fission life should be long. The latter requires the friction to be strong as is known from Kramers limit [29,58], while the former requires neutron-rich compound nuclei to be initially formed because of the smallness of the neutron separation energy which accelerates the cooling. Anyhow, it is desired that the excitation energy of the initial compound nuclei formed be as low as possible, so that the potential pocket or the fission barrier is quickly formed due to the low starting temperature. This is more or less our common knowledge, especially learned from GSI experiments. On the other hand, as the Smoluchowski equation describes the diffusion of the probability from the initial distribution given by the touching configuration of the incident ions, the probability which diffuses into the compact configuration, i.e., inside the fission barrier, to emerge later is larger for a larger diffusion coefficient $D=T/\mu\beta$. This requires the initial temperature to be large: i.e., the initial excitation energy is desired to be high. Briefly speaking, the initial excitation energy of compound nuclei is required to be lower for larger residue probabilities in the later stage of the reaction and to be higher for larger diffusion into the inside of the barrier in the early stage of the reaction, compromising of which thus gives rise to the optimum excitation energy. This is a new mechanism never discussed before and is extremely important for the synthesis of the superheavy elements. In the present calculations we use the shell correction energy calculated with the Woods-Saxon potential, and discuss the nuclide with $Z=114$ and $N=184$, but if there were another large shell correction minimum such as predicted by the microscopic model elsewhere in the nuclear chart, the present model, of course, could apply, though the residue cross section depends on the absolute value of the shell correction energy. That is, the larger the correction energy is, the larger the residue cross section is. It also depends on the Z value of the compound nuclei formed, naturally the smaller for the larger Z due to higher extra fusion barriers. And it should be noted that absolute values of residue cross sections depend on the average neutron separation energy $\langle B_n\rangle$ over a few emissions as shown in Fig. 9. Thus, availability of neutron-rich beam and/or target is strongly desirable and promising for the synthesis of the superheavy elements. The time evolution of the probability distributions during the damping in the initial kinetic energy just after the touching is being studied with the Langevin equation in the multidimensional space of deformation without assuming the immediate damping of the present calculations and will be reported in the forthcoming paper. Cases with mass-asymmetric combinations of incident ions are also being investigated in the multidimensional space.

ACKNOWLEDGMENTS

The authors thank Dr. D. Guerreau for his encouragement since the early stages of this work. The authors acknowledge useful discussions with Dr. G. Münzenberg, Dr. K.-H. Schmidt, and Dr. Yu. Ts. Oganessian. This work was partly supported by the Grant-in-Aid for Scientific Research on the Priority Areas (No. 08213101) of the Ministry of Education, Science, Sports and Culture in Japan, and the Hirao Taro Foundation of the Konan University Association for Academic Research.

APPENDIX A: THE DERIVATION OF THE FREE ENERGY FROM SINGLE-PARTICLE LEVELS

The temperature dependence of the shell correction energy is deduced by calculating the free energy and its variation from the smoothed one which is expected to correspond to LDM energy

$$V_{\rm shell}(x,T)=F(x,T)-\langle F(x,T)\rangle,$$

$$F(x,T)=E(x,T)-T\cdot S(x,T),$$

$$E(x,T)=\Sigma_i\epsilon_i\cdot f_i,$$

$$S(x,T)=-\Sigma_i\{-f_i\ \ln\ f_i-(\overline{f_i})\ln(\overline{f_i})\}, \tag{A1}$$

where ϵ_i is the energy of the ith single-particle level which is calculated with the Woods-Saxon potential with a deformation [5], $f_i=f(\epsilon_i,T)$ is the Fermi distribution function at temperature T, and $\overline{f}(\epsilon_i,T)=1-f(\epsilon_i,T)$. The second term of Eq. (A1) is the smoothed one, following Strutinski's prescription,

$$\langle F(x,T)\rangle=\langle E(x,T)\rangle-T\cdot\langle S(x,T)\rangle,$$

$$\langle E(x,T)\rangle=\int g(\epsilon)\epsilon f(\epsilon)d\epsilon,$$

$$\langle S(x,T)\rangle=\int d\epsilon g(\epsilon)\{-f(\epsilon)\ln\ f(\epsilon)-[\overline{f}(\epsilon)]\ln[\overline{f}(\epsilon)]\}, \tag{A2}$$

where $g(\epsilon)$ is the averaged level density,

$$g(\epsilon)=\Sigma_i\frac{1}{\sqrt{2\pi}\sigma}e^{-(\epsilon-\epsilon_i)^2/2\sigma^2}, \tag{A3}$$

with a value of σ suitably chosen so that the shell structure effect is smeared out. The temperature dependence of the pairing energy is assumed to be the same as that of the shell correction energy.

APPENDIX B: STATISTICAL CODE SIMDEC

A new Monte Carlo simulation code SIMDEC is developed for analysis of the statistical decaying process of compound nucleus [54]. In this appendix, we explain the calculation procedure of SIMDEC and compare the results by the code SIMDEC with the experimental data and the results by another simulation code.

In the paper, the fission decay width Γ_f is calculated by the diffusion model, not by the statistical model. In the calculation of the cooling curve we use the code SIMDEC and the temperature variation by the particle emissions is calculated with $\Gamma_f=0$.

In the code SIMDEC, the time duration $\Delta t^{(i)}$ from the ith stage to the $(i+1)$th one by particle emission is estimated from the total width $\Gamma^{(i)}$ calculated at the ith disintegration stage [60],

$$\Delta t^{(i)}=-\frac{\hbar}{\Gamma^{(i)}}\ln R \quad (0<R<1),$$

$$\Gamma^{(i)}=\sum_{k=n,p,\alpha,\gamma}\Gamma_k^{(i)}+\overline{\Gamma}_f^{(i)}, \tag{B1}$$

where k stands for the index of disintegration channels, i.e., neutron, proton, alpha, and gamma channels. R is a random number. The mean fission width in each disintegration step $\overline{\Gamma}_f^{(i)}$ is calculated from the delay property of fission [28,29].

The time-dependent fission width is assumed to have the following factor:

$$\Gamma_f(t)=f(t)\Gamma_f^{\mathrm{BW}},$$

$$f(t)=1\Big/\left(1+\exp\left\{\frac{t-t_c}{d}\right\}\right), \tag{B2}$$

where Γ_f^{BW} is the Bohr-Wheeler fission width given by the transition state method [59], and t_c and d are parameters to realize the delay time of fission and are determined consistently with the solution in the Langevin equation study [28].

In the actual calculations, the average value of fission width $\overline{\Gamma}_f^{(i)}$ in each disintegration step is determined as follows. At the first step, we find the half lifetime t_1 for various disintegrations, which satisfies

$$\frac{1}{\hbar}\int_0^{t_1}\left\{\sum_{j=n,p,\alpha,\gamma}\Gamma_j^{(1)}+\Gamma_f(t)\right\}dt=1. \tag{B3}$$

This equation means that the system disintegrates with unit probability until t_1. The average value $\overline{\Gamma}_f^{(1)}$ used in the first step of disintegration can be obtained by

$$\overline{\Gamma}_f^{(1)}=\frac{1}{t_1}\int_0^{t_1}\Gamma_f(t)dt. \tag{B4}$$

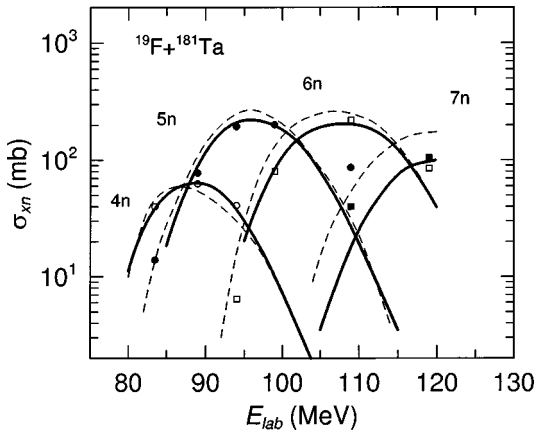

FIG. 15. Excitation function for evaporation residue cross section for the ^{181}Ta (^{19}F, xn) reaction. Open circles, solid circles, and open squares represent the measured cross sections for $4n$, $5n$, and $6n$ channels, respectively. The data originate from Hinde *et al.* (1982) [63] and Charity *et al.* (1986) [64]. The dashed curves are standard predictions for the cross section with the code ALICE. The thick solid curves correspond to the excitation function as calculated from our code SIMDEC.

At the second step, we find the time t_2 in the same way,

$$\frac{1}{\hbar}\int_{t_1'}^{t_2}\left\{\sum_{j=n,p,\alpha,\gamma}\Gamma_j^{(2)}+\Gamma_f(t)\right\}dt=1; \tag{B5}$$

here, the lower limit of the integral t_1' is equal to $\Delta t^{(1)}$ estimated by Eq. (B1), and $\Gamma_f(t)$ is averaged over the time interval (t_1',t_2) to get $\overline{\Gamma}_f^{(2)}$. The same process is done for successive steps, for example, $t_2'=t_1'+\Delta t^{(2)}+\cdots$.

In each time interval thus determined, $(0,t_1'),(t_1',t_2'),\ldots$, the decay channel is specified by using a random number according to the weight of $\Gamma_k^{(i)}$ and $\overline{\Gamma}_f^{(i)}$.

The particle binding energy is calculated from the Möller's mass table [5]. The angular momentum transfer for particle emission is treated precisely. For the nuclear level density, use is made of the formula by Gilbert and Cameron [61] with Grossjean and Feldmeier's correction [62] at low energies to estimate the γ-ray width correctly. The fission barrier $B_f(T)$ in SIMDEC is composed of the parts of the droplet model and temperature-dependent shell and pairing correction:

$$B_f(T)=B_f^{\mathrm{DM}}(T)-(\delta U_{\mathrm{sh}}^{\mathrm{g.s.}}+\delta U_{\mathrm{pair}}^{\mathrm{g.s.}})\exp\{-a^2T/E_d\}, \tag{B6}$$

$$B_f^{\mathrm{DM}}(T)=B_f^{\mathrm{DM}}(T=0)(1-\xi T^2). \tag{B7}$$

The results by the code SIMDEC are compared with the experimental data and the calculations given by another simulation code to confirm its validity. For example, the data for the ^{181}Ta (^{19}F, xn) reaction [63,64] are analyzed and are compared with the results by the code ALICE [65] as shown in Fig. 15.

[1] V. M. Strutinski, Nucl. Phys. **A95**, 420 (1967).
[2] V. M. Strutinski, Nucl. Phys. **A122**, 1 (1968).
[3] W. D. Myers and W. J. Swiatecki, Nucl. Phys. **81**, 1 (1966).
[4] W. D. Myers and W. J. Swiatecki, Ark. Fys. **36**, 343 (1967).
[5] P. Möller, J. R. Nix, W. D. Myers, and W. J. Swiatecki, At. Data Nucl. Data Tables **59**, 185 (1995).
[6] Z. Patyk and A. Sobiczewski, in *Low Energy Nuclear Dynamics*, edited by Yu.Ts. Oganessian, W. von Oertzen, and R. Kalpakcheva (World Scientific, Singapore, 1995), p. 313.
[7] U. Mosel and W. Greiner, Z. Phys. **222**, 261 (1969).
[8] S. G. Nilsson, C. F. Wycech, A. Sobiczewski, Z. Szymański, S. Wycech, C. Gustafson, I.-L. Lamm, P. Möller, and B. Nilsson, Nucl. Phys. **A131**, 1 (1969).
[9] K. Rutz, M. Bender, T. Bürvenich, T. Schilling, P.-G. Reinhard, J. A. Maruhn, and W. Greiner, Phys. Rev. C **56**, 238 (1997).
[10] S. Ćwiok, J. Dobaczewski, P.-H. Heenen, P. Magierski, and W. Nazarewicz, Nucl. Phys. **A611**, 211 (1996).
[11] P. Armbruster, Annu. Rev. Nucl. Sci. **35**, 135 (1985).
[12] G. Münzenberg, Rep. Prog. Phys. **51**, 57 (1988).
[13] Yu. Ts. Oganessian and Y. A. Lazarev, in *Treatise on Heavy-Ion Science*, edited by D. A. Bromley (Plenum, New York, 1985), pp. 3–251.
[14] S. Hofmann *et al.*, Z. Phys. A **354**, 229 (1996).
[15] Yu. Ts. Oganessian, Nucl. Phys. **A488**, 65c (1988).
[16] H. Gaeggeler *et al.*, Z. Phys. A **289**, 415 (1979).
[17] Yu. Ts. Oganessian, *Classical and Quantum Mechanical Aspects in Heavy Ion Collision, Lecture Notes in Physics*, Vol. 33 (Springer-Verlag, Heidelberg, 1975), p. 221.
[18] Yu. Ts. Oganessian *et al.*, Radiochim. Acta **37**, 113 (1984).
[19] G. Münzenberg *et al.*, Z. Phys. A **309**, 89 (1982).
[20] S. Hofmann *et al.*, Z. Phys. A **350**, 277 (1995); **350**, 281 (1995).
[21] W. Greiner, Int. J. Mod. Phys. E **5**, 1 (1995).
[22] PIAFE Collaboration, in *Low Energy Nuclear Dynamics* [6], pp. 30–43.
[23] H. Nifenecker (private communication).
[24] T. Sikkeland, J. Maly, and D. F. Lebeck, Phys. Rev. **169**, 1000 (1968).
[25] A. N. Andreyev *et al.*, Z. Phys. A **345**, 389 (1993).
[26] A. Gavron *et al.*, Phys. Rev. C **35**, 579 (1987).
[27] D. J. Hinde, D. Hilscher, and H. Rossner, Nucl. Phys. **A502**, 497c (1989).
[28] T. Wada, Y. Abe, and N. Carjan, Phys. Rev. Lett. **70**, 3538 (1993).
[29] Y. Abe, S. Ayik, P.-G. Reinhard, and E. Suraud, Phys. Rep. **275**, 49 (1996).
[30] K.-H. Schmidt and W. Morawek, Rep. Prog. Phys. **54**, 949 (1991).
[31] W. Reisdorf and M. Schädel, Z. Phys. A **343**, 47 (1992).
[32] Y. Aritomo, T. Wada, M. Ohta, and Y. Abe, Phys. Rev. C **55**, R1011 (1997).
[33] T. Wada, Y. Aritomo, T. Tokuda, M. Ohta, and Y. Abe, Nucl. Phys. **A616**, 446c (1997).
[34] Y. Abe, Y. Aritomo, T. Wada and M. Ohta, J. Phys. G **23**, 1275 (1997).
[35] Y. Aritomo, K. Okazaki, T. Wada, M. Ohta, and Y. Abe, in *Proceedings of Tours Symposium on Nuclear Physics III*, edited by M. Arnould, M. Lewitowicz, Yu. Ts. Oganessian, M. Ohta, H. Utsunomiya, and T. Wada, AIP Conf. Proc. No. 425 (AIP, New York, 1998), p. 61.
[36] C. W. Gardiner, *Handbook of Stochastic Methods* (Springer-Verlag, Berlin, 1990).
[37] J. P. Blocki, H. Feldmeier, and W. J. Swiatecki, Nucl. Phys. **A459**, 145 (1986).
[38] P. Fröbrich, Phys. Rep. **116**, 337 (1984).
[39] C. E. Aguiar, V. C. Barbosa, R. Donangelo, and S. R. Souza, Nucl. Phys. **A491**, 301 (1989).
[40] C. E. Aguiar, V. C. Barbosa, and R. Donangelo, Nucl. Phys. **A517**, 205 (1990).
[41] W. J. Swiatecki, Phys. Scr. **24**, 113 (1981).
[42] W. J. Swiatecki, Nucl. Phys. **A376**, 275 (1982).
[43] S. Bjørnholm and W. J. Swiatecki, Nucl. Phys. **A391**, 471 (1982).
[44] P. Paul and M. Thoennessen, Annu. Rev. Nucl. Part. Sci. **44**, 65 (1994).
[45] H. A. Weidenüller and J.-S. Zhang, Phys. Rev. C **29**, 879 (1984).
[46] R. Vandenbosch and J. R. Huizenga, *Nuclear Fission* (Academic Press, New York, 1973).
[47] R. Bass, *Nuclear Reactions with Heavy Ions* (Springer-Verlag, Berlin, 1980).
[48] J. Maruhn and W. Greiner, Z. Phys. **251**, 431 (1972).
[49] K. Sato, A. Iwamoto, K. Harada, S. Yamaji, and S. Yoshida, Z. Phys. A **288**, 383 (1978).
[50] K.-H. Schmit, Nucl. Phys. **A488**, 47c (1988).
[51] X. Campi and S. Stringari, Z. Phys. A **309**, 239 (1983).
[52] R. W. Hasse and W. D. Myers, *Geometrical Relationships of Macroscopic Nuclear Physics* (Springer-Verlag, Berlin, 1988).
[53] H. J. Krappe, in ''Proceedings of the International Workshop on Dynamical Aspects of Nuclear Fission,'' Smolenice, CSFR, 1991, JINR Dubna, Report No. E7-92-95, p. 51.
[54] M. Ohta, Y. Aritomo, T. Tokuda, and Y. Abe, in *Proceedings of Tours Symposium on Nuclear Physics II*, edited by H. Utsunomiya, M. Ohta, J. Galin, and G. Münzenberg (World Scientific, Singapore, 1995), p. 480.
[55] A. V. Ignatyuk, G. N. Smirenkin, and A. S. Tishin, Sov. J. Nucl. Phys. **21**, 255 (1975).
[56] J. Töke and W. J. Swiatecki, Nucl. Phys. **A372**, 141 (1981).
[57] V. Weisskopf, Phys. Rev. **52**, 295 (1937).
[58] H. A. Kramers, Physica (Utrecht) **7**, 284 (1940).
[59] N. Bohr and J. A. Wheeler, Phys. Rev. **56**, 426 (1939).
[60] A. Gavron *et al.*, Phys. Rev. C **35**, 579 (1987).
[61] A. Gilbert and A. G. W. Cameron, Can. J. Phys. **43**, 1446 (1965).
[62] M. K. Grossjean and H. Feldmeier, Nucl. Phys. **A444**, 113 (1985).
[63] D. J. Hinde, J. R. Leigh, J. O. Newton, W. Galster, and S. Sie, Nucl. Phys. **A385**, 109 (1982).
[64] R. J. Charity *et al.*, Nucl. Phys. **A457**, 441 (1986).
[65] F. Pasil, Oak Ridge National Laboratory Report No. ORNL/TM-6054, 1977.